

# Quantum scars in many-body systems

Andrea Pizzi,<sup>1,2,\*</sup> Bertrand Evrard,<sup>3</sup> Ceren B. Dag,<sup>4,2</sup> and Johannes Knolle<sup>5,6,7</sup>

<sup>1</sup>*Cavendish Laboratory, University of Cambridge, Cambridge CB3 0HE, United Kingdom*

<sup>2</sup>*Department of Physics, Harvard University, Cambridge, Massachusetts 02138, USA*

<sup>3</sup>*Laboratoire Matériaux et Phénomènes Quantiques, Université Paris Cité, 75013 Paris, France*

<sup>4</sup>*ITAMP, Center for Astrophysics, Harvard & Smithsonian, Cambridge, Massachusetts 02138, USA*

<sup>5</sup>*Department of Physics, Technische Universität München TQM, James-Frank-Straße 1, 85748 Garching, Germany*

<sup>6</sup>*Munich Center for Quantum Science and Technology (MCQST), 80799 Munich, Germany*

<sup>7</sup>*Blackett Laboratory, Imperial College London, London SW7 2AZ, United Kingdom*

Chaos makes isolated systems of many interacting particles quickly thermalize and forget about their past. Here, we show that quantum mechanics hinders chaos in many-body systems: although the quantum eigenstates are thermal and strongly entangled, exponentially many of them are scarred, that is, have an enlarged weight along underlying classical unstable periodic orbits. Scarring makes the system more likely to be found on an orbit it was initialized on, retaining a memory of its past and thus weakly breaking ergodicity, even at long times and despite the system being fully thermal. We demonstrate the ubiquity of quantum scarring in many-body systems by considering a large family of spin models, including some of the most popular ones from condensed matter physics. Our findings, at hand for modern quantum simulators, prove structure in spite of chaos in many-body quantum systems.

Understanding and controlling many-body quantum systems out of equilibrium is a key challenge of modern physics. Left to their isolated dynamics, as becoming increasingly possible in ever improving quantum computers and simulators [1–6], these systems tend to quickly relax to thermal equilibrium, effectively forgetting about their past in the spirit of ergodicity [7–9]. This fate is as universal as tame, and underpinning it is the seemingly chaotic nature of the many-body Hamiltonian. Indeed, the statistical properties of the system’s eigenvalues and eigenvectors are in many respect similar to those of certain random matrices [10].

It is known for single-particle systems, however, that chaos can be hindered by quantum scarring [11–13]. This is the phenomenon whereby the quantum wavefunction is enhanced along underlying classical unstable periodic orbits (UPOs). Scarred eigenstates are less random than chaos would suggest, increasing the chances of finding the system on a UPO it was prepared on and challenging the notion of ergodicity [13, 14]. Scarring has long been known within single-particle quantum chaos, but its generalization to many-body quantum systems, whose study requires modern quantum simulators and more advanced numerical tools, has remained virtually unexplored [15].

Here, we show that scarring is ubiquitous in many-body systems. For a large family of spin chains, we find that exponentially many eigenstates are enhanced along the UPOs of the associated classical dynamics. Initializing the system on a UPO enhances the probability of finding it on the same UPO at later times. Even in the middle of the spectrum, where entanglement is close to maximal and the eigenstate thermalization hypothesis (ETH) fulfilled [16], we show that the eigenstates are less chaotic than expected and ergodicity is weakly broken.

Our work adds quantum scarring to the (short) list of mechanisms yielding nontrivial effects in many-body quantum systems out of equilibrium, such as integrability [17, 18],

many-body localization [19–22], Hilbert space fragmentation [23, 24], and non-thermal eigenstates in an otherwise chaotic spectrum [25–29]. All these rely on an explicit or emergent partial integrability. By contrast, scarring establishes a deviation from chaos in the thermal eigenstates of generic non-integrable many-body systems, where one would least expect it.

A remark on nomenclature is due. Growing attention has been recently devoted to certain many-body quantum systems hosting a few eigenstates which violate ETH and are weakly entangled [26–29]. While these have been dubbed “quantum many-body scars”, there is no evidence that they are in fact scars, because they could not be related to UPOs in a chaotic phase space [15, 27, 30][31]. To avoid suggesting a link between such non-thermal eigenstates and our work, we will refrain from talking about “many-body quantum scars” and simply use “quantum scars”, emphasizing the many-body context in which they occur.

*Model, classical dynamics, and UPOs* — Consider a chain of  $N$  spin  $s$  particles subject to a magnetic field and nearest-neighbor interactions ( $\hbar = 1$ )

$$\hat{H} = \sum_{j=1}^N \left( \boldsymbol{\mu} \cdot \hat{\mathbf{s}}_j + \frac{1}{s} \hat{\mathbf{s}}_j \mathbf{J} \hat{\mathbf{s}}_{j+1} \right), \quad (1)$$

where  $\hat{\mathbf{s}}_j^2 = s(s+1)$ ,  $\hat{\mathbf{s}}_j \mathbf{J} \hat{\mathbf{s}}_{j+1} = \sum_{\alpha,\beta=x,y,z} \hat{s}_j^\alpha J_{\alpha\beta} \hat{s}_{j+1}^\beta$ ,  $\boldsymbol{\mu} \cdot \hat{\mathbf{s}}_j = \sum_{\alpha=x,y,z} \mu_\alpha \hat{s}_j^\alpha$ , and periodic boundary conditions are assumed. This Hamiltonian is very general, e.g., it describes *any* homogeneous spin 1/2 chain with nearest-neighbor interactions, including many prototypical models of condensed matter physics. For instance, the Ising model with both transverse and longitudinal (integrability-breaking) fields is obtained for  $\mu_y = 0$  and  $\mathbf{J} = J_{zz} \mathbf{z} \otimes \mathbf{z}$ , yielding  $\hat{H} = \frac{1}{2} \sum_j (\mu_x \hat{\sigma}_j^x + \mu_z \hat{\sigma}_j^z + J_{zz} \hat{\sigma}_j^z \hat{\sigma}_{j+1}^z)$ , with  $\hat{\sigma}_j^{x,z}$  standard Pauli operators. The Heisenberg, XX, and XXZ models are obtained in a similar way. The normalization  $s^{-1}$  in

front of the interaction in Eq. (1) ensures a well-defined limit  $s \rightarrow \infty$ , for which the spins can be described as classical rotors  $\{\mathbf{s}_j\}$ , with  $|\mathbf{s}_j|^2 = 1$  and dynamics [32]

$$\frac{d\mathbf{s}_j}{dt} = [\boldsymbol{\mu} + \mathbf{J}(\mathbf{s}_{j-1} + \mathbf{s}_{j+1})] \times \mathbf{s}_j. \quad (2)$$

The nonlinear dynamics in Eq. (2) is generally chaotic and aperiodic. There are however special families of spin configurations for which the dynamics is periodic instead, see Fig. 1(a). One is that of the translationally invariant (TI) states, in which all the spins are aligned,  $\{\mathbf{s}_j\} = (s, s, s, s, \dots)$ . Another, for  $N$  multiple of 4, is that of the interaction suppressing (IS) states, in which the spins flip at every other site,  $\{\mathbf{s}_j\} = (+s, +s, -s, -s, +s, +s, -s, -s, \dots)$ . These states are special in that the classical dynamics in Eq. (2) does not destroy their nature: a TI state remains such, owing to translational invariance, and a IS state remains such, because  $\mathbf{s}_{j-1} + \mathbf{s}_{j+1} = 0$  and the interaction is suppressed. The dynamics from these states is fully specified by the dynamics of just one spin, say  $\mathbf{s}$ , namely

$$\frac{d\mathbf{s}}{dt} = \begin{cases} (\boldsymbol{\mu} + 2\mathbf{J}\mathbf{s}) \times \mathbf{s} & \text{for TI states} \\ \boldsymbol{\mu} \times \mathbf{s} & \text{for IS states} \end{cases}. \quad (3)$$

The vector  $\mathbf{s}$  lives on the surface of a sphere, and its Hamiltonian dynamics must be periodic, like any in two dimensions [33].

The many-body dynamics from a TI or IS state will also be periodic but, crucially, generally unstable: a slight perturbation that breaks the TI or IS character of the initial condition leads through chaos to a highly unpredictable and non-periodic trajectory exploring the many-body phase space ergodically. For the IS states and  $|\mathbf{J}| \ll |\boldsymbol{\mu}|$ , we compute all the Lyapunov exponents *analytically* [34], showing that the IS states are indeed unstable for all models but trivial ones (e.g.,  $\lambda = 0$  for the Ising model in a longitudinal field). The TI and IS states thus constitute two manifolds of UPOs within the classical many-body phase space, Fig. 1(b). The existence of continuous manifolds of UPOs, rather than isolated UPOs, is a favourable factor for scarring [14]. Note that other such manifolds exist [35].

As first shown for quantum billiards [13], scarring can be expected when  $\lambda\omega < 1$ , with  $\lambda$  the Lyapunov exponent of the UPO and  $T = 2\pi/\omega$  its period. That is, scars are expected when chaos, acting on a timescale  $\sim \lambda^{-1}$ , does not prevent a classical trajectory nearby an UPO to return to its neighborhood after one period. In Fig. 1(c) we compute  $\lambda/\omega$  for some cases of interest. The IS is unstable in all the considered parameter range, with  $\lambda/\omega \sim |\mathbf{J}|/|\boldsymbol{\mu}|$ , suggesting that scarring can be enhanced by simply increasing the strength of the field  $|\boldsymbol{\mu}|$ . The TI state also has  $\lambda/\omega < 1$ , but becomes stable ( $\lambda = 0$ ) for small  $|\mathbf{J}|$ . In the following, we consider TI and IS states only when they are unstable ( $\lambda > 0$ ), which is paramount when talking about quantum scars [13].

*Quantum scars* — Let us go back to the quantum many-body problem  $\hat{H} |E_n\rangle = E_n |E_n\rangle$ . The effective size of the

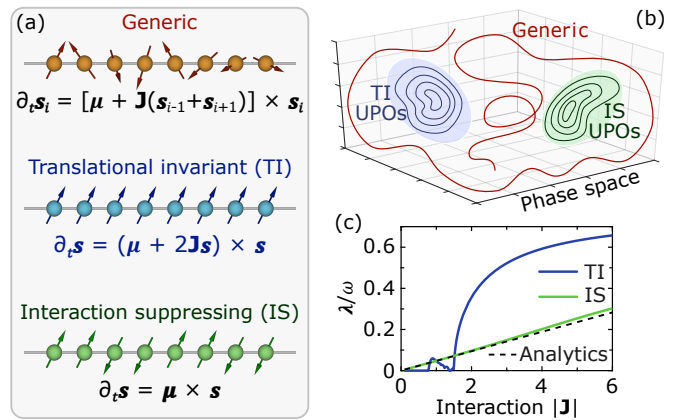


FIG. 1. **Classical spin dynamics and unstable periodic orbits.** (a) The dynamics of a classical spin chain is generally chaotic, but yields unstable periodic orbits (UPOs) for the TI states, with aligned spins (blue), and for the IS states, with spins alternating every other site (green). (b) The TI states and IS states form two-dimensional manifolds of UPOs within the highly-dimensional phase space. (c) Quantum scarring is favoured for  $\lambda/\omega < 1$ , with  $\lambda$  the Lyapunov exponent of the UPO and  $\omega$  its frequency. This condition holds throughout the whole considered parameter regime, and especially for small  $|\mathbf{J}|/|\boldsymbol{\mu}|$ . In (c) we considered the Ising model with  $\boldsymbol{\mu} = (2.4, 0, 0.4)$ ,  $N = 100$ , and the UPOs through  $\mathbf{s} = \mathbf{y}$ . The Lyapunov exponent is computed numerically from the monodromy matrix [36], and analytically (dashed line) for the IS states and  $|\mathbf{J}| \ll |\boldsymbol{\mu}|$  [34].

Hilbert space is reduced by exploiting the symmetries of the Hamiltonian and of the TI and IS states [37]. The eigenstates, attained by exact diagonalization, fulfill the ETH and are characterized by an extensive bipartite entanglement entropy, see Fig. 2(a,b). To look for scarring we project the eigenstates onto the classical phase space. Each point  $\{\mathbf{s}_i\}$  of the phase space is associated to a product state  $|\{\mathbf{s}_i\}\rangle = |\mathbf{s}_1\rangle \otimes |\mathbf{s}_2\rangle \otimes \dots \otimes |\mathbf{s}_N\rangle$ , with  $\mathbf{s}_i$  the orientation of the  $i$ -th quantum spin,  $(\mathbf{s}_i \cdot \hat{\mathbf{s}}_i) |\mathbf{s}_i\rangle = s |\mathbf{s}_i\rangle$ ; the projection of a wavefunction  $|\psi\rangle$  on the classical phase space reads  $Q = |\langle \{\mathbf{s}_i\} | \psi \rangle|^2$ .

The high dimensionality of the classical phase space makes visualizing  $Q$  generally complicated. Nonetheless, we are mostly interested in projections along the UPOs, which lie on two-dimensional manifolds parametrized by a polar angle  $\theta$  and an azimuth  $\phi$ . For a few eigenstates in the middle of the spectrum, in Fig. 2(c) we show the projection  $Q$  on the manifolds of TI and IS states. Indeed, the many-body eigenstates display an enhanced projection along certain UPOs, that is, quantum scars. The degree of scarring, as well as which UPOs are responsible for it, varies from eigenstate to eigenstate. Scarring is particularly remarkable for the IS manifold: not only are all the considered eigenstates in the middle of the spectrum,  $E_n \approx 0$ , but the whole IS manifold is, because any IS state yields  $\langle \{\mathbf{s}_i\} | \hat{H} | \{\mathbf{s}_i\} \rangle = 0$ . That is, the enhanced overlap with an UPO cannot be due to that UPO being at a special energy, which makes scarring even more surprising, in analogy with quantum billiards in which the classical orbits are all at the same energy  $\frac{p^2}{2m}$  [11].

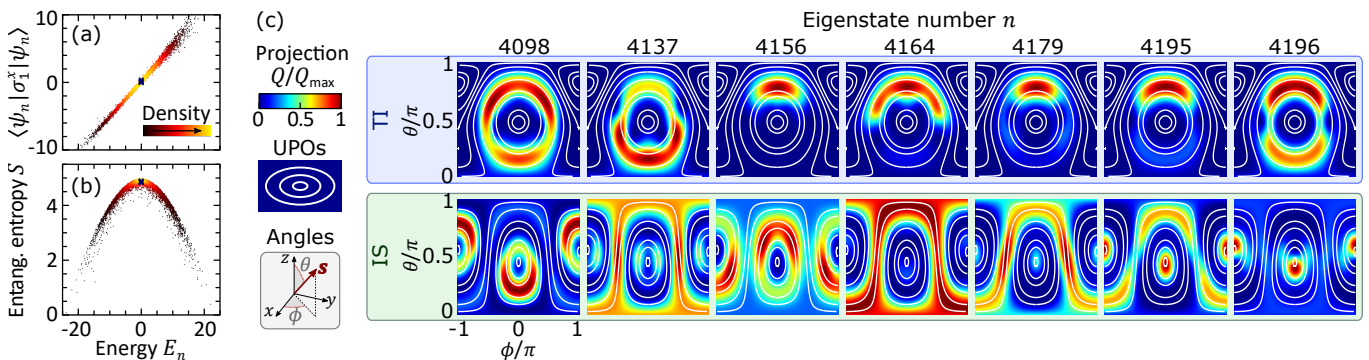


FIG. 2. **Quantum scars in many-body spin chains.** (a,b) The many-body eigenstates  $|E_n\rangle$  are fully thermal: the expectation value of local observables, e.g.,  $\langle E_n | \hat{\sigma}_1^x | E_n \rangle$ , only depends on the energy [16], as does the bipartite entanglement entropy  $S$ , which is extensive,  $S \sim N$ . (c) Projection of selected eigenstates  $|E_n\rangle$  onto the TI and IS manifolds of the classical phase space (top and bottom, respectively). The many-body eigenstates are scarred, that is, enhanced along certain UPOs (white lines). The considered eigenstates are marked in (a,b) by crosses, and sit in the middle of the thermal spectrum. Here, we considered the Ising model with  $\boldsymbol{\mu} = (2.4, 0, 0.4)$ ,  $J_{zz} = -1.8$ , and  $N = 16$ .

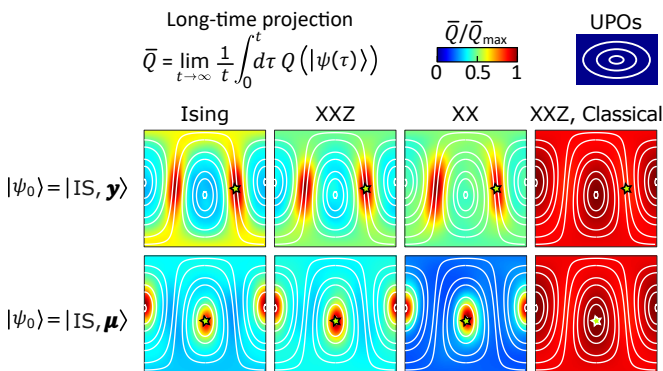


FIG. 3. **Weak ergodicity breaking from quantum scarring.** Time-averaged projection  $Q(|\psi(t)\rangle)$  over the manifold of IS states, for various models and initial conditions. In the top row, the system is initialized on the IS UPO aligned along  $\mathbf{y}$  ( $\phi = \theta = \pi/2$ , marked by a star), and is more likely to be found on the same UPO at long times. In the bottom row, the system is initialized on the IS UPO aligned along  $\boldsymbol{\mu}$  (also marked by a star), and is more likely to be found there at long times. That is, the system retains some information on its initial condition and weakly breaks ergodicity. This is a quantum effect: the classical projection [34], shown for the XXZ model, is insensitive to the initial condition and almost uniform. Here, we considered  $N = 20$  and  $\boldsymbol{\mu} = (2.4, 0, 0.4)$ , and chose  $\mathbf{J}$  ensuring that the system is fully thermal:  $J_{zz} = -1.8$  for the Ising model,  $J_{xx} = J_{yy} = -0.4$  and  $J_{zz} = -1.8$  for the XXZ model, and  $J_{xx} = J_{yy} = -1.4$  for the XX model.

The eigenstates shown in Fig. 2 are selected to showcase scarring in its various shapes and colors. But by no means does scarring require cherry picking: as for billiards [11], most eigenstates are to some extent scarred, which we also show for the XX and XXZ models in [34]. Indeed, while the thermal spectrum makes the system quickly equilibrate, the scarring of exponentially many eigenstates leaves a mark on the long-time dynamics. In analogy to single-particle quantum chaos [13], preparing the system on a UPO increases the probability of finding it on the same UPO at later times. This

effect is shown in Fig. 3 by considering two initial conditions: the IS state with axis  $\mathbf{y}$ , namely  $|\psi_0\rangle = \otimes_{i=1}^N |\nu_i \mathbf{y}\rangle$ , and the IS state with axis  $\boldsymbol{\mu}$ , namely  $|\psi_0\rangle = \otimes_{i=1}^N |\nu_i \boldsymbol{\mu} / |\boldsymbol{\mu}|\rangle$ , with  $\{\nu_i\} = (+ + - - + + - - \dots)$ . For both we numerically integrate the Schrödinger dynamics and compute the time-averaged projection  $\bar{Q} = \lim_{t \rightarrow \infty} \frac{1}{t} \int_0^t d\tau Q(|\psi(\tau)\rangle)$  on the manifold of IS states. For the Ising, XX, and XXZ models in a field, we observe that the system is more likely to be found on the UPO it started from, even long after thermalization.

We emphasize that this effect is not due to the initial condition overlapping with a few non-thermal eigenstates [26], but to most of the thermal eigenstates being scarred. This is a genuinely quantum effect: due to ergodicity, a classical ensemble prepared nearby an IS UPO will at long times spread uniformly across the phase space at  $E = 0$ , in a way that does not depend on the specific initial condition, see Fig. 3. By striking contrast, it is more likely to find the quantum system on the UPO it started from. In other words, scarring makes the quantum system remember its past better than a classical system would, in a rare example of weak ergodicity breaking. We use the adjective *weak* because, while the enhancement of the phase-space projection on the UPOs is large in relative terms, it is small in absolute terms, possibly scaling as  $Q \sim N e^{-O(N)}$ , e.g.,  $Q_{\max} \sim 5 \times 10^{-4}$  in Fig. 2 and  $\bar{Q}_{\max} \sim 3 \times 10^{-5}$  in Fig. 3. Indeed, scarring should be seen as a small albeit measurable correction to the picture of thermalization in isolated quantum systems [7, 9], not contradicting paradigms such as the ETH [16].

**Conclusions** — Analysing a very broad family of spin chains, including *any* uniform spin-1/2 chain with nearest-neighbor interactions, our work proves the ubiquity of quantum scarring in many-body systems. The  $s \rightarrow \infty$  classical dynamics in Eq. (2) scars the quantum system all the way down to the deep-quantum limit of  $s = \frac{1}{2}$ . Scarring enhances the eigenstates  $|E_n\rangle$  along certain UPOs and makes a system better remember its past, curbing chaos even in fully thermal and non-integrable many-body systems.



Our predictions can be straightforwardly verified in state-of-the-art quantum simulators for spin Hamiltonians [2–6], opening new possibilities for the experimental observation of scars [38–42]. In particular, by repeatedly preparing a product state, letting it evolve, and measuring it in a different basis, one should be able to show that the system is more likely to be found on the UPO it was prepared on (Fig. 3), which is a direct consequence of quantum scarring. Our work also opens many avenues for theoretical research, posing questions regarding the role of lattice geometry and interaction range, the fate of scarring in the limits  $s \rightarrow \infty$  and  $N \rightarrow \infty$ , and possibilities with other fermionic and bosonic particles. Realizing that the atypical eigenstates in so-called “many-body quantum scars” are in fact not scars is not merely a matter of terminology [30]: it opens the door to a whole new field of research, that of scars – genuine scars [11] – in many-body systems, and paves the way to a better understanding of the quantum-classical correspondence.

**Acknowledgements.** We thank A. Buchleitner, C. Castelnovo, A. Das, I. Kaminer, S. I. Mistakidis, S. Moudgalya, A. Nunnenkamp, N. Rivera, and N. Yao for insightful discussions on related work and comments on the manuscript. A. P. acknowledges support by Trinity College Cambridge.

---

\* [ap2076@cam.ac.edu](mailto:ap2076@cam.ac.edu)

- [1] C. Gross and I. Bloch, Quantum simulations with ultracold atoms in optical lattices, *Science* **357**, 995 (2017).
- [2] R. Blatt and C. F. Roos, Quantum simulations with trapped ions, *Nature Physics* **8**, 277 (2012).
- [3] J. Zhang, G. Pagano, P. W. Hess, A. Kyprianidis, P. Becker, H. Kaplan, A. V. Gorshkov, Z.-X. Gong, and C. Monroe, Observation of a many-body dynamical phase transition with a 53-qubit quantum simulator, *Nature* **551**, 601 (2017).
- [4] H. Bernien, S. Schwartz, A. Keesling, H. Levine, A. Omran, H. Pichler, S. Choi, A. S. Zibrov, M. Endres, M. Greiner, *et al.*, Probing many-body dynamics on a 51-atom quantum simulator, *Nature* **551**, 579 (2017).
- [5] C. Monroe, W. C. Campbell, L.-M. Duan, Z.-X. Gong, A. V. Gorshkov, P. W. Hess, R. Islam, K. Kim, N. M. Linke, G. Pagano, *et al.*, Programmable quantum simulations of spin systems with trapped ions, *Reviews of Modern Physics* **93**, 025001 (2021).
- [6] X. Mi, M. Ippoliti, C. Quintana, A. Greene, Z. Chen, J. Gross, F. Arute, K. Arya, J. Atalaya, R. Babbush, *et al.*, Time-crystalline eigenstate order on a quantum processor, *Nature* **601**, 531 (2022).
- [7] A. Polkovnikov, K. Sengupta, A. Silva, and M. Vengalattore, Colloquium: Nonequilibrium dynamics of closed interacting quantum systems, *Reviews of Modern Physics* **83**, 863 (2011).
- [8] J. Eisert, M. Friesdorf, and C. Gogolin, Quantum many-body systems out of equilibrium, *Nature Physics* **11**, 124 (2015).
- [9] L. D’Alessio, Y. Kafri, A. Polkovnikov, and M. Rigol, From quantum chaos and eigenstate thermalization to statistical mechanics and thermodynamics, *Advances in Physics* **65**, 239 (2016).
- [10] Y. Y. Atas, E. Bogomolny, O. Giraud, and G. Roux, Distribution of the ratio of consecutive level spacings in random matrix ensembles, *Physical review letters* **110**, 084101 (2013).
- [11] E. J. Heller, Bound-state eigenfunctions of classically chaotic hamiltonian systems: scars of periodic orbits, *Physical Review Letters* **53**, 1515 (1984).
- [12] M. V. Berry, Quantum scars of classical closed orbits in phase space, *Proceedings of the Royal Society of London. A. Mathematical and Physical Sciences* **423**, 219 (1989).
- [13] L. Kaplan, Scars in quantum chaotic wavefunctions, *Nonlinearity* **12**, R1 (1999).
- [14] L. Kaplan and E. Heller, Linear and nonlinear theory of eigenfunction scars, *Annals of Physics* **264**, 171 (1998).
- [15] B. Evrard, A. Pizzi, S. I. Mistakidis, and C. B. Dag, Quantum many-body scars from unstable periodic orbits, *arXiv preprint arXiv:2401.06848* (2024).
- [16] M. Rigol, V. Dunjko, and M. Olshanii, Thermalization and its mechanism for generic isolated quantum systems, *Nature* **452**, 854 (2008).
- [17] M. Rigol, V. Dunjko, V. Yurovsky, and M. Olshanii, Relaxation in a completely integrable many-body quantum system: an ab initio study of the dynamics of the highly excited states of 1d lattice hard-core bosons, *Physical review letters* **98**, 050405 (2007).
- [18] B. Evrard, A. Pizzi, S. I. Mistakidis, and C. B. Dag, Quantum scars and regular eigenstates in a chaotic spinor condensate, *Physical Review Letters* **132**, 020401 (2024).
- [19] A. Pal and D. A. Huse, Many-body localization phase transition, *Physical Review B—Condensed Matter and Materials Physics* **82**, 174411 (2010).
- [20] F. Alet and N. Laflorencie, Many-body localization: An introduction and selected topics, *Comptes Rendus Physique* **19**, 498 (2018).
- [21] D. A. Abanin, E. Altman, I. Bloch, and M. Serbyn, Colloquium: Many-body localization, thermalization, and entanglement, *Reviews of Modern Physics* **91**, 021001 (2019).
- [22] D. Sels and A. Polkovnikov, Dynamical obstruction to localization in a disordered spin chain, *Physical Review E* **104**, 054105 (2021).
- [23] P. Sala, T. Rakovszky, R. Verresen, M. Knap, and F. Pollmann, Ergodicity breaking arising from hilbert space fragmentation in dipole-conserving hamiltonians, *Physical Review X* **10**, 011047 (2020).
- [24] V. Khemani, M. Hermele, and R. Nandkishore, Localization from hilbert space shattering: From theory to physical realizations, *Physical Review B* **101**, 174204 (2020).
- [25] S. Moudgalya, N. Regnault, and B. A. Bernevig, Entanglement of exact excited states of affleck-kennedy-lieb-tasaki models: Exact results, many-body scars, and violation of the strong eigenstate thermalization hypothesis, *Physical Review B* **98**, 235156 (2018).
- [26] C. J. Turner, A. A. Michailidis, D. A. Abanin, M. Serbyn, and Z. Papić, Weak ergodicity breaking from quantum many-body scars, *Nature Physics* **14**, 745 (2018).
- [27] W. W. Ho, S. Choi, H. Pichler, and M. D. Lukin, Periodic orbits, entanglement, and quantum many-body scars in constrained models: Matrix product state approach, *Physical review letters* **122**, 040603 (2019).
- [28] M. Serbyn, D. A. Abanin, and Z. Papić, Quantum many-body scars and weak breaking of ergodicity, *Nature Physics* **17**, 675 (2021).
- [29] S. Moudgalya, B. A. Bernevig, and N. Regnault, Quantum many-body scars and hilbert space fragmentation: a review of exact results, *Reports on Progress in Physics* **85**, 086501 (2022).
- [30] A. Michailidis, C. Turner, Z. Papić, D. Abanin, and M. Serbyn, Slow quantum thermalization and many-body revivals from



- mixed phase space, *Physical Review X* **10**, 011055 (2020).
- [31] In fact, when a link to a classical phase space was attempted, the non-thermal eigenstates of the PXP model were shown to relate to regular regions of the phase space [27, 30]. Accordingly, they should be called “regular eigenstates” instead of “scars” [30].
- [32] L. Landau and E. Lifshitz, On the theory of the dispersion of magnetic permeability in ferromagnetic bodies, *Phys. Z. Sowjetunion* **8**, 101 (1935).
- [33] S. H. Strogatz, *Nonlinear dynamics and chaos with student solutions manual: With applications to physics, biology, chemistry, and engineering* (CRC press, 2018).
- [34] See Supplemental Material.
- [35] In fact, the IS states are part of a broader manifold of periodic orbits, namely  $\{\mathbf{s}_j\} = (+\mathbf{s}_1, +\mathbf{s}_2, -\mathbf{s}_1, -\mathbf{s}_2, +\mathbf{s}_1, +\mathbf{s}_2, -\mathbf{s}_1, -\mathbf{s}_2, \dots)$ , that evolve according to  $\frac{d\mathbf{s}_{1,2}}{dt} = \boldsymbol{\mu} \times \mathbf{s}_{1,2}$ .
- [36] G. Contopoulos, *Order and chaos in dynamical astronomy*, Vol. 21 (Springer, 2002).
- [37] The IS and TI states, as well as the Hamiltonian, are invariant with respect to translations by 4 sites and with respect to a mirror reflection. As customary in the numerical simulation of quantum many-body systems, we exploit these symmetries to reduce the effective size of the Hilbert space, which remains however exponentially large, e.g., of size 720, 8356, and 105376 for  $N = 12, 16$ , and 20, respectively.
- [38] D. Wintgen and A. Hönig, Irregular wave functions of a hydrogen atom in a uniform magnetic field, *Physical review letters* **63**, 1467 (1989).
- [39] S. Sridhar, Experimental observation of scarred eigenfunctions of chaotic microwave cavities, *Physical review letters* **67**, 785 (1991).
- [40] J. Stein and H.-J. Stöckmann, Experimental determination of billiard wave functions, *Physical review letters* **68**, 2867 (1992).
- [41] T. Fromhold, P. Wilkinson, F. Sheard, L. Eaves, J. Miao, and G. Edwards, Manifestations of classical chaos in the energy level spectrum of a quantum well, *Physical review letters* **75**, 1142 (1995).
- [42] P. Wilkinson, T. Fromhold, L. Eaves, F. Sheard, N. Miura, and T. Takamasu, Observation of ‘scarred’ wavefunctions in a quantum well with chaotic electron dynamics, *Nature* **380**, 608 (1996).

# Supplementary Information for “Quantum scars in many-body systems”

Andrea Pizzi, Bertrand Evrard, Ceren B. Dag, and Johannes Knolle

This Supplementary Information is devoted to technical derivations and complementary details. It is structured as follows. In Section I, we present some complementary results supporting the ubiquity of quantum scarring in many-body systems. In Section II we develop the tools needed to compute the Lyapunov exponent of the IS states, namely we perform a zero-th order Floquet expansion in a frame precessing around the external magnetic field  $\mu$ . In Section III we compute the Lyapunov exponent for the IS UPOs in the limit of small  $|J|/|\mu|$ . In Section IV we provide a few more details on computing classical phase-space projections.

## I) UBIQUITY OF SCARS

To show the ubiquity of quantum scarring in many body systems in Fig. S1 we generalize Fig. 2 from the main text, considering the Ising, XXZ, and XX models in a field. Moreover, we do not consider a selection of eigenstates, but simply the 10 eigenstates in the middle of the spectrum (that is composed of 8356 eigenstates overall). The Ising model is like that in the main text, the XXZ model reads

$$H = \frac{1}{2} \sum_j [\mu \cdot \sigma_j + J_{xx} (\sigma_j^z \sigma_{j+1}^z + \sigma_j^z \sigma_{j+1}^z) + J_{zz} \sigma_j^z \sigma_{j+1}^z], \quad (\text{S1})$$

and the XX model reads

$$H = \frac{1}{2} \sum_j [\mu \cdot \sigma_j + J_{xx} (\sigma_j^z \sigma_{j+1}^z + \sigma_j^z \sigma_{j+1}^z)]. \quad (\text{S2})$$

The specific values of the parameters are the same as in Fig. 2 in the main text, and ensure that the system is well thermalized. The expectation value  $\langle E_n | \sigma_1^x | E_n \rangle$  and the bipartite entanglement entropy  $S$  for the eigenstates  $|E_n\rangle$  is shown in Fig. S1, and confirms thermalization. The projection of the 10 central eigenstates onto the manifold of IS UPOs is shown in Fig. S1(b). To various extents, most eigenstates show some structure that correlates with the UPOs, that is, quantum scarring.

By contrast, in Fig. S2 we show the projection of random states onto the IS states, and see no noteworthy structure. The random states are built as  $|\psi_{\text{rnd}}\rangle = \sum_c \alpha_c |c\rangle$ , where  $|c\rangle$  are the states of the computational basis. The states  $|c\rangle$  are the states of the computational basis within the same symmetry subsector considered in the main text, meaning invariant under translations by 4 sites and mirror symmetry. The coefficients  $\alpha_c$  are obtained as follows. First, they are drawn as independent real random numbers between 0 and 1; Second, they are renormalized such that  $\sum_c \alpha_c^2 = 1$ ; Third and last, a random phase is added. Because the states  $|c\rangle$  are within the symmetry subsector of interest, and the random states still do not show noteworthy structure in the projections, we conclude that the structure of the projection of the eigenstates cannot be simply attributed to the symmetry subsector being separated by the rest of the Hilbert space, and must be due to genuine quantum scarring.

Next, we show that within the considered (and exponentially large) symmetry sector, most eigenstates are scarred. Let us focus on scarring in the manifold of IS states. A strongly scarred eigenstate is one with  $Q \sim Q_{\text{max}}$  along some UPO. That is, we should look at the average  $Q/Q_{\text{max}}$  over an UPO, which we denote  $\oint_{\text{UPO}} Q/Q_{\text{max}}$ , and look for the UPO that maximizes it. For a wavefunction  $|\psi\rangle$  with projection  $Q$  we thus introduce the following figure of merit for scarring

$$S = \max_{\text{UPOs}} \left[ \oint_{\text{UPO}} Q/Q_{\text{max}} \right]. \quad (\text{S3})$$

We compute  $S$  for all the eigenstates, and also for an ensemble of the random wavefunctions  $|\psi_{\text{rnd}}\rangle$  introduced above. We then introduce the scarring fraction  $\chi$  as the probability that, picking one eigenstate  $|E_n\rangle$  at random, and drawing one random wavefunction  $|\psi_{\text{rnd}}\rangle$ , the quantity  $S$  is larger for the eigenstate than for the random function. As well, we introduce the number of scarred eigenstates  $N_{\text{scarred}}$  as the number of eigenstates that have a  $S$  larger than the average  $S$  of the random wavefunctions.

We consider various models (with parameters as in Fig. S1) and system sizes  $N$ . For the Ising model, we find  $\chi \approx 78\%$ ,  $77\%$ , and  $78\%$  and  $N_{\text{scarred}} = 59, 576$ , and  $6888$  for  $N = 8, 12$ , and  $16$ , respectively. For the XXZ model, we find  $\chi \approx 83\%$ ,  $79\%$ , and  $76\%$  and  $N_{\text{scarred}} = 69, 606$ , and  $6613$  for  $N = 8, 12$ , and  $16$ , respectively. For the XX model, we find  $\chi \approx 82\%$ ,  $77\%$ , and  $74\%$  and  $N_{\text{scarred}} = 68, 582$ , and  $6446$  for  $N = 8, 12$ , and  $16$ , respectively. That is, the probability of scarring  $\chi$  remains large

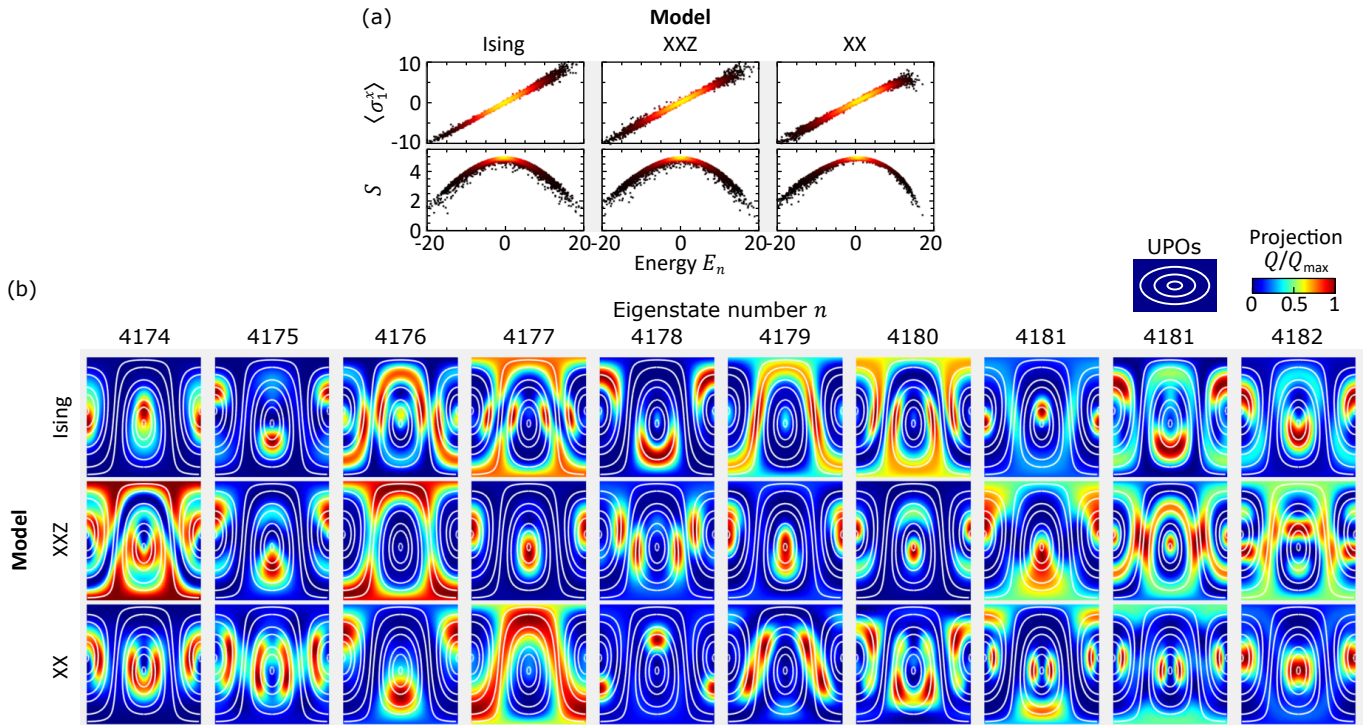


Fig. S1. **Ubiquity of quantum scars.** (a) Expectation value  $\langle E_n | \sigma_1^x | E_n \rangle$  and bipartite entanglement entropy  $S$  for the eigenstates  $|E_n\rangle$  of the Ising, XXZ, and XX models. (b) Projection over the manifold of IS states of 10 consecutive eigenstates taken in the middle of the spectrum. Most of the eigenstates appear scarred, to some variable extent, by the UPOs. Here,  $N = 16$ .

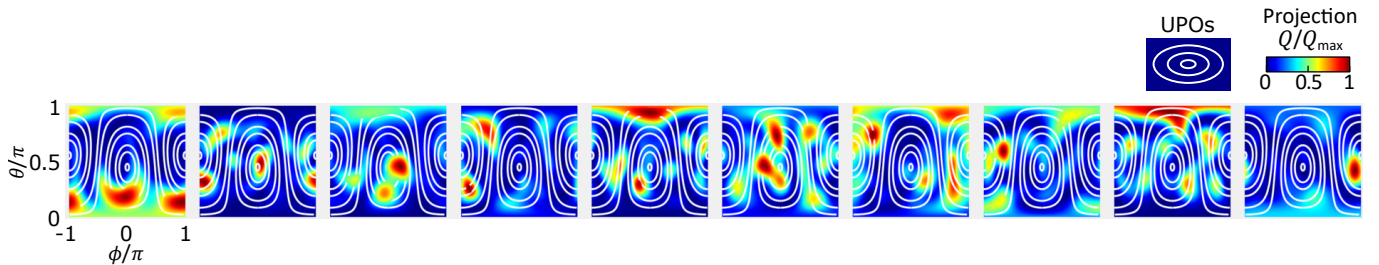


Fig. S2. **Phase-space projection of random states.** Projection  $Q$  of random states, for  $N = 16$ . Random states do not show any noteworthy structure, and in particular not in relation to the underlying classical UPOs.

and approximately constant (or only slowly decaying) with the system size  $N$ , and the number of scarred eigenstates  $N_{\text{scarred}}$  grows exponentially with the system size. Note that quantifying scarring is not an easy task, and that there is no unique way of doing it. The analysis above succeeds in indicating that scarring affects most of the eigenstates, but for instance does not consider that certain eigenstates are scarred by multiple UPOs. There is thus room for a systematic quantitative analysis of scarring in many-body systems, which goes however beyond the scope of this work.

## II) ZERO-TH ORDER FLOQUET EXPANSION

In the frame precessing around  $\mu$  at the frequency of the IS UPOs, namely  $\omega = \frac{2\pi}{T} = |\mu|$ , the Hamiltonian reads

$$\hat{H}_{\text{rot}}(t) = \frac{1}{s} \sum_{i=1}^N \hat{s}_i \mathbf{R}^{-1}(\omega t) \mathbf{J} \mathbf{R}(\omega t) \hat{s}_{i+1}. \quad (\text{S4})$$



The matrix  $\mathbf{R}$  can be written using Rodrigues formula

$$\mathbf{R}(\omega t) = \mathbf{I} + \sin(\omega t)\mathbf{u}_\times + [1 - \cos(\omega t)](\mathbf{u}_\times)^2, \quad (\text{S5})$$

$$= \mathbf{u} \otimes \mathbf{u} + \sin(\omega t)\mathbf{u}_\times + \cos(\omega t)(\mathbf{I} - \mathbf{u} \otimes \mathbf{u}), \quad (\text{S6})$$

where  $\mathbf{u}_\times \mathbf{a} = \mathbf{u} \times \mathbf{a}$ ,  $\mathbf{u} = \boldsymbol{\mu}/|\boldsymbol{\mu}|$ , and where we used  $\mathbf{I} + (\mathbf{u}_\times)^2 = \mathbf{u} \otimes \mathbf{u}$ . The zero-th order Floquet expansion corresponds to substituting  $\hat{H}_{\text{rot}}(t)$  with its time average,  $\hat{H} = \frac{1}{T} \int_0^T dt \hat{H}_{\text{rot}}(t)$ . That is,

$$\hat{H} = \frac{1}{s} \sum_{i=1}^N \hat{s}_i \bar{\mathbf{J}} \hat{s}_{i+1}, \quad (\text{S7})$$

with

$$\bar{\mathbf{J}} = \frac{1}{T} \int_0^T dt \mathbf{R}^{-1}(\omega t) \mathbf{J} \mathbf{R}(\omega t), \quad (\text{S8})$$

$$= \int_0^1 dx [\mathbf{u} \otimes \mathbf{u} \mathbf{J} \mathbf{u} \otimes \mathbf{u} - \sin^2(2\pi x) \mathbf{u}_\times \mathbf{J} \mathbf{u}_\times + \cos^2(2\pi x) (\mathbf{I} - \mathbf{u} \otimes \mathbf{u}) \mathbf{J} (\mathbf{I} - \mathbf{u} \otimes \mathbf{u})], \quad (\text{S9})$$

$$= \mathbf{u} \otimes \mathbf{u} (\mathbf{u} \mathbf{J} \mathbf{u}) - \frac{1}{2} \mathbf{u}_\times \mathbf{J} \mathbf{u}_\times + \frac{1}{2} (\mathbf{I} - \mathbf{u} \otimes \mathbf{u}) \mathbf{J} (\mathbf{I} - \mathbf{u} \otimes \mathbf{u}). \quad (\text{S10})$$

Using the properties of the cross product we find

$$\mathbf{u}_\times \mathbf{J} \mathbf{u}_\times = (\mathbf{I} - \mathbf{u} \otimes \mathbf{u}) (\mathbf{u} \mathbf{J} \mathbf{u} - \text{Tr}\{\mathbf{J}\}) + (\mathbf{I} - \mathbf{u} \otimes \mathbf{u}) \mathbf{J} (\mathbf{I} - \mathbf{u} \otimes \mathbf{u}), \quad (\text{S11})$$

and thus

$$\bar{\mathbf{J}} = \mathbf{u} \otimes \mathbf{u} (\mathbf{u} \mathbf{J} \mathbf{u}) + \frac{1}{2} (\mathbf{u} \otimes \mathbf{u} - \mathbf{I}) (\mathbf{u} \mathbf{J} \mathbf{u} - \text{Tr}\{\mathbf{J}\}), \quad (\text{S12})$$

$$= \mathbf{u} \otimes \mathbf{u} \frac{1}{2} (3\mathbf{u} \mathbf{J} \mathbf{u} - \text{Tr}\{\mathbf{J}\}) - \mathbf{I} \frac{1}{2} (\mathbf{u} \mathbf{J} \mathbf{u} - \text{Tr}\{\mathbf{J}\}). \quad (\text{S13})$$

It will prove useful to further characterize the matrix  $\bar{\mathbf{J}}$ . Its eigenvectors are  $\mathbf{u}$  and any two vectors orthogonal to it, with eigenvalues

$$\lambda_1 = \mathbf{u} \mathbf{J} \mathbf{u}, \quad \lambda_2 = \lambda_3 = -\frac{1}{2} (\mathbf{u} \mathbf{J} \mathbf{u} - \text{Tr}\{\mathbf{J}\}), \quad (\text{S14})$$

and so

$$\det(\bar{\mathbf{J}}) = \frac{1}{4} (\mathbf{u} \mathbf{J} \mathbf{u}) (\mathbf{u} \mathbf{J} \mathbf{u} - \text{Tr}\{\mathbf{J}\})^2, \quad (\text{S15})$$

$$\text{Tr}\{\bar{\mathbf{J}}\} = \text{Tr}\{\mathbf{J}\}. \quad (\text{S16})$$

Moreover, we note that

$$[\mathbf{u} \otimes \mathbf{u} (3\mathbf{u} \mathbf{J} \mathbf{u} - \text{Tr}\{\mathbf{J}\}) - 2(\mathbf{u} \mathbf{J} \mathbf{u}) \mathbf{I}] \bar{\mathbf{J}} = (\mathbf{u} \mathbf{J} \mathbf{u}) (\mathbf{u} \mathbf{J} \mathbf{u} - \text{Tr}\{\mathbf{J}\}) \mathbf{I}, \quad (\text{S17})$$

and thus find the adjoint  $\text{Adj}(\bar{\mathbf{J}})$  such that  $(\text{Adj}(\bar{\mathbf{J}})) \bar{\mathbf{J}} = \det(\bar{\mathbf{J}}) \mathbf{I}$ , namely

$$\text{Adj}(\bar{\mathbf{J}}) = \frac{1}{4} (\mathbf{u} \mathbf{J} \mathbf{u} - \text{Tr}\{\mathbf{J}\}) [\mathbf{u} \otimes \mathbf{u} (3\mathbf{u} \mathbf{J} \mathbf{u} - \text{Tr}\{\mathbf{J}\}) - 2(\mathbf{u} \mathbf{J} \mathbf{u}) \mathbf{I}]. \quad (\text{S18})$$

### III) LYAPUNOV EXPONENT

We compute the classical Lyapunov exponent associated to the IS UPOs, in which the spin direction flips every other spin,  $\{s_j\} = (+s, +s, -s, -s, +s, +s, -s, -s, \dots)$ . Various values of  $s$  correspond to various UPOs, and we should thus use  $s$  as a parameter, a tag of the considered UPO. Computing the Lyapunov exponent with respect to a periodic orbit can be complicated, but by moving to the frame precessing around the magnetic field  $\boldsymbol{\mu}$ , and assuming that  $|\boldsymbol{\mu}|/|\mathbf{J}| \gg 1$ , we transform the UPO

into a fixed point of the dynamics, which considerably simplifies the computation of the Lyapunov exponent. In such frame the classical spin dynamics reads

$$\frac{d\mathbf{s}_i}{dt} = (\bar{\mathbf{J}}(\mathbf{s}_{i-1} + \mathbf{s}_{i+1})) \times \mathbf{s}_i. \quad (\text{S19})$$

We want to study the evolution of small perturbation on top of the UPO. Let us say  $\mathbf{s}_i = \nu_i \mathbf{s} + \boldsymbol{\epsilon}_i$ , with  $\{\nu_i\} = (+ + - - + + - - \dots)$  and  $\boldsymbol{\epsilon}_i$  a small perturbation of order  $\epsilon \ll 1$ . Because  $\nu_{i-1} + \nu_{i+1} = 0$ , then  $|\mathbf{s}_{i-1} + \mathbf{s}_{i+1}| \sim \epsilon$ , and thus at first order in  $\epsilon$  we can consider

$$\frac{d\boldsymbol{\epsilon}_i}{dt} \approx -\nu_i \mathbf{s} \times [\bar{\mathbf{J}}(\boldsymbol{\epsilon}_{i-1} + \boldsymbol{\epsilon}_{i+1})], \quad (\text{S20})$$

$$= \nu_i \mathbf{M}(\boldsymbol{\epsilon}_{i-1} + \boldsymbol{\epsilon}_{i+1}), \quad (\text{S21})$$

where  $\mathbf{M} = -\mathbf{s} \times \bar{\mathbf{J}}$ . We perform a Fourier transformation

$$f_k = \sum_j e^{-ikj} f_j, \quad f_j = \frac{1}{N} \sum_k e^{ikj} f_k, \quad (\text{S22})$$

and, noting that  $\nu_j = -\frac{1+i}{2} e^{i\pi/2j} - \frac{1-i}{2} e^{-i\pi/2j}$ , get

$$(\nu_j(\boldsymbol{\epsilon}_{j-1} + \boldsymbol{\epsilon}_{j+1}))_k = \sum_j e^{-ikj} \nu_j (\boldsymbol{\epsilon}_{j-1} + \boldsymbol{\epsilon}_{j+1}), \quad (\text{S23})$$

$$= -\sum_j e^{-ikj} \left( \frac{1+i}{2} e^{i\pi/2j} + \frac{1-i}{2} e^{-i\pi/2j} \right) (\boldsymbol{\epsilon}_{j-1} + \boldsymbol{\epsilon}_{j+1}), \quad (\text{S24})$$

$$= -\sum_j \left( \frac{1+i}{2} e^{-i(k-\pi/2)j} + \frac{1-i}{2} e^{-i(k+\pi/2)j} \right) (\boldsymbol{\epsilon}_{j-1} + \boldsymbol{\epsilon}_{j+1}), \quad (\text{S25})$$

$$= -(1+i) \cos\left(k - \frac{\pi}{2}\right) \boldsymbol{\epsilon}_{k-\pi/2} - (1-i) \cos\left(k + \frac{\pi}{2}\right) \boldsymbol{\epsilon}_{k+\pi/2}, \quad (\text{S26})$$

$$= -(1+i) \sin(k) \boldsymbol{\epsilon}_{k-\pi/2} + (1-i) \sin(k) \boldsymbol{\epsilon}_{k+\pi/2}. \quad (\text{S27})$$

The eigenproblem reads

$$\frac{d\boldsymbol{\epsilon}_k}{dt} = \lambda \boldsymbol{\epsilon}_k = -(1+i) \sin(k) \mathbf{M} \boldsymbol{\epsilon}_{k-\pi/2} + (1-i) \sin(k) \mathbf{M} \boldsymbol{\epsilon}_{k+\pi/2}, \quad (\text{S28})$$

and iterating it once we get

$$\lambda^2 \boldsymbol{\epsilon}_k = -(1+i) \sin(k) \cos(k) \mathbf{M}^2 (-(1+i) \boldsymbol{\epsilon}_{k-\pi} + (1-i) \boldsymbol{\epsilon}_k) - (1-i) \sin(k) \cos(k) \mathbf{M}^2 (-(1+i) \boldsymbol{\epsilon}_k + (1-i) \boldsymbol{\epsilon}_{k+\pi}), \quad (\text{S29})$$

$$= 2i \mathbf{M}^2 \sin(2k) \boldsymbol{\epsilon}_{k+\pi} \quad (\text{S30})$$

Iterating once more we can close the equation, getting

$$\lambda^4 \boldsymbol{\epsilon}_k = -4 \mathbf{M}^4 \sin^2(2k) \boldsymbol{\epsilon}_k. \quad (\text{S31})$$

We find that  $\mathbf{M}^2$  has one vanishing eigenvalue and two degenerate eigenvalues  $\alpha = -\mathbf{s}[\text{adj}(\bar{\mathbf{J}})]\mathbf{s}$ . Thus,

$$\lambda_{k,m} = \sqrt{2\alpha |\sin(2k)|} e^{i\frac{\pi}{4} + im\frac{\pi}{2}}, \quad (\text{S32})$$

for  $m = 1, 2, 3, 4$ . That is, we have managed to find all the  $6N$  eigenvalues of the problem, of which  $2N$  vanish due to the two-dimensional space of spins (instead of three-dimensional). The instability exponent  $\lambda$  is the largest of the real parts of the eigenvalues, obtained for  $k = \frac{\pi}{4}$  and giving  $\lambda^2 = |\alpha| = |\mathbf{s}[\text{adj}(\bar{\mathbf{J}})]\mathbf{s}|$ . Using the expression found in Eq. (S18) we get

$$\lambda^2 = \frac{1}{4} |(\mathbf{u} \mathbf{J} \mathbf{u} - \text{Tr}\{\mathbf{J}\}) [(\mathbf{u} \cdot \mathbf{s})^2 (3\mathbf{u} \mathbf{J} \mathbf{u} - \text{Tr}\{\mathbf{J}\}) - 2\mathbf{u} \mathbf{J} \mathbf{u}]|. \quad (\text{S33})$$

For instance, for the Ising model in a field we get

$$\lambda^2 = \frac{1}{4} J^2 u_x^2 [(1 - 3u_z^2)(\mathbf{u} \cdot \mathbf{s})^2 + 2u_z^2]. \quad (\text{S34})$$

#### IV) CLASSICAL FIDELITY

The overlap of a classical state  $|\{\mathbf{s}'_j\}\rangle$  onto a point  $\{\mathbf{s}_j\}$  of the classical phase space reads

$$Q = |\langle\{\mathbf{s}_j\}|\{\mathbf{s}'_j\}\rangle|^2 = \prod_j |\langle\mathbf{s}_j|\mathbf{s}'_j\rangle|^2 = \prod_j \left(\frac{1 + \mathbf{s}'_j \cdot \mathbf{s}_j}{2}\right)^{2s}. \quad (\text{S35})$$

Consider a point  $\{\mathbf{s}_j\}$  of the classical phase space. A perturbation of this point is obtained by rotating each spin by an angle  $\theta_j$  drawn at random from a Gaussian distribution with standard deviation  $\Delta \ll 1$ . Considering many such perturbations we obtain an ensemble of phase-space points  $\{\mathbf{s}_j^{(r)}\}$ , with  $r = 1, 2, \dots, R$ , that are closely localized around the reference point  $\{\mathbf{s}_j\}$ . By classically time evolving the ensemble, we obtain the corresponding classical time-averaged projection

$$\bar{Q}_c(\{\mathbf{s}_j\}) = \frac{1}{R} \sum_{r=1}^R \lim_{t \rightarrow \infty} \frac{1}{t} \int_0^t d\tau \prod_j \left(\frac{1 + \mathbf{s}_j \cdot \mathbf{s}_j^{(r)}(\tau)}{2}\right)^{2s}. \quad (\text{S36})$$

Note that  $\bar{Q}_c(\{\mathbf{s}_j\})$  is exponentially small in both  $N$  and  $s$ . Thus, the larger  $N$  and  $s$  and the larger is the  $R$  that guarantees convergence. In Fig. 3 we consider  $s = 1/2$ , for which a good convergence is obtained for  $R = 2 \times 10^5$  samples.